Behavioral/Cognitive

Hippocampus–Prefrontal Coupling Regulates Recognition Memory for Novelty Discrimination

Cong Wang,[1,2] Teri M. Furlong,[2,3,4] Peter G. Stratton,[1] Conrad C. Y. Lee,[1,2,5] Li Xu,[1] Sam Merlin,[2,6] Chris Nolan,[1,2] Ehsan Arabzadeh,[2,5] Roger Marek,[1,2] and Pankaj Sah[1,2,7]

[1]Queensland Brain Institute, The University of Queensland, Brisbane 4072, Queensland, Australia, [2]Australian Research Council Centre of Excellence for Integrative Brain Function, Clayton 3800, Victoria, Australia, [3]Neuroscience Research Australia, Sydney 2031, New South Wales, Australia, [4]School of Medical Sciences, The University of New South Wales, Sydney 2052, New South Wales, Australia, [5]John Curtin School of Medical Research, Australian National University, Canberra 2601, Australian Capital Territory, Australia, [6]School of Science, Western Sydney University, Campbelltown 2560, New South Wales, Australia, and [7]Joint Center for Neuroscience and Neural Engineering, and Department of Biology, Southern University of Science and Technology, Shenzhen 518055, Guangdong Province, People's Republic of China

Recognition memory provides the ability to distinguish familiar from novel objects and places, and is important for recording and updating events to guide appropriate behavior. The hippocampus (HPC) and medial prefrontal cortex (mPFC) have both been implicated in recognition memory, but the nature of HPC–mPFC interactions, and its impact on local circuits in mediating this process is not known. Here we show that novelty discrimination is accompanied with higher theta activity (4–10 Hz) and increased c-Fos expression in both these regions. Moreover, theta oscillations were highly coupled between the HPC and mPFC during recognition memory retrieval for novelty discrimination, with the HPC leading the mPFC, but not during initial learning. Principal neurons and interneurons in the mPFC responded more strongly during recognition memory retrieval compared with learning. Optogenetic silencing of HPC input to the mPFC disrupted coupled theta activity between these two structures, as well as the animals' (male Sprague Dawley rats) ability to differentiate novel from familiar objects. These results reveal a key role of monosynaptic connections between the HPC and mPFC in novelty discrimination via theta coupling and identify neural populations that underlie this recognition memory-guided behavior.

Key words: **context; hippocampus; memory; novelty; prefrontal cortex; recognition**

Significance Statement

Many memory processes are highly dependent on the interregional communication between the HPC and mPFC via neural oscillations. However, how these two brain regions coordinate their oscillatory activity to engage local neural populations to mediate recognition memory for novelty discrimination is poorly understood. This study revealed that the HPC and mPFC theta oscillations and their temporal coupling is correlated with recognition memory-guided behavior. During novel object recognition, the HPC drives mPFC interneurons to effectively reduce the activity of principal neurons. This study provides the first evidence for the requirement of the HPC–mPFC pathway to mediate recognition memory for novelty discrimination and describes a mechanism for how this memory is regulated.

Introduction

Recognition memory is a type of episodic memory that facilitates discrimination of novel from previously encountered objects and experiences, and is fundamental in recording and updating the state of the external environment, guiding appropriate behavior (Warburton and Brown, 2015). The neural circuits that mediate this memory have been investigated using molecular markers of neural activity combined with lesion and/or inactivation of the regions that are found to be active. This experimental approach in rodents has shown that object recognition is accompanied by upregulated expression of immediate early gene (IEG) markers of neural activity, such as c-Fos, in the hippocampus (HPC) and perirhinal cortex (PRh; Wan et al., 1999; Tanimizu et al., 2018).

Received May 23, 2021; revised Sep. 5, 2021; accepted Sep. 27, 2021.

Author contributions: C.W., T.M.F., R.M., and P.S. designed research; C.W., T.M.F., C.C.Y.L., L.X., S.M., and R.M. performed research; C.W., T.M.F., C.N., and P.G.S. analyzed data; C.W., T.M.F., P.G.S., C.C.Y.L., C.N., E.A., R.M. and P.S. wrote the paper.

This work is supported by grants from the Australian National Health and Research Council and by Australian Research Council Grant CE140100007. We thank J. Lynch, A. Woodruff, R. Tweedale, and P. Sedlak for comments on the manuscript. We also thank R. Sullivan for the protocol and help in immunohistology. In addition, we thank the Queensland Brain Institute for support in viral expression imaging using LSM 510 and Axio Imagers Blue at the Advanced Microscopy Facility.

The authors declare no competing financial interests.

Correspondence should be addressed to Pankaj Sah at pankaj.sah@uq.edu.au or Roger Marek at r.marek@uq.edu.au.

https://doi.org/10.1523/JNEUROSCI.1202-21.2021

Lesion or chemical inactivation of these regions impairs recognition memory (Clark et al., 2000; Baker and Kim, 2002; Hammond et al., 2004; Iwamura et al., 2016; Miranda et al., 2018). Thus, current models suggest that recognition memory is critically dependent on the HPC and PRh (Cohen et al., 2013), two regions that integrate information about "what" happens "where" (Eichenbaum, 2000). Complementing animal studies, the HPC is active during recognition memory tasks in humans, and patients with selective damage to the HPC show impairments in recognition memory (Manns et al., 2003; Smith et al., 2014; Merkow et al., 2015).

The participation of the HPC and PRh in object memory processing is well known, but these regions are also extensively connected with the medial prefrontal cortex (mPFC; Siapas et al., 2005; Hoover and Vertes, 2007), a region that has a central role in decision-making and memory consolidation. However, whether the mPFC has a role in recognition memory is under considerable debate (Barker et al., 2007; Warburton and Brown, 2010, 2015; Barbosa et al., 2013; Morici et al., 2015; Barker et al., 2017; Tanimizu et al., 2018; Tuscher et al., 2018). Interestingly, network activity in the mPFC has been found to synchronize with that in the HPC during memory recall (Jones and Wilson, 2005; Xia et al., 2017), but whether such synchronous activity is required for object recognition is not known.

To address these questions, we used the novel object recognition (NOR) task (Bevins and Besheer, 2006) to study the functional connections between the HPC and mPFC during object recognition memory. By performing simultaneous electrophysiological recordings in the HPC and mPFC, we show that NOR is driven by temporally coupled theta frequency (4–10 Hz) activity in these two regions. These theta oscillations are led by the HPC, and optogenetic silencing of HPC input to the mPFC disrupts coupled theta activity and novelty discrimination. Our results provide direct evidence for the involvement of the HPC and mPFC in NOR, and identifies the synaptic connections and network mechanism required for NOR.

Materials and Methods

Subjects. Male Sprague Dawley rats (age, 5–12 weeks) were obtained from the Animal Resources Center (Perth, Western Australia, Australia) and housed in groups of two to four in OptiRAT cages or standard cages under a 12 h light/dark cycle (light phase, 7:00 A.M. to 7:00 P.M.), with food and water provided *ad libitum*. All experiments were performed during the light phase. All procedures were performed in accordance with the Australian Code for the Care and Use of Animals for Scientific Purposes and the Australian Code for the Responsible Conduct of Research and approved by the Animal Ethics Committees of the University of Queensland and the University of New South Wales.

VersaDrive construction. VersaDrives (NeuraLynx) with two/four/eight independently movable drives were assembled in-house. Tetrodes were prepared by folding a platinum-iridium (17.78 μm; California Fine Wire) or nichrome wire (17.78 μm; A-M Systems) twice to form a bundle and then twisting the bundle together with a tetrode spinner (NeuraLynx). Guiding tubes (inner diameter, 99.7 μm; Polymicro Technologies and Molex) were used to support the tetrodes. To enhance the signal-to-noise ratio (SNR), a plating procedure was performed on the tetrode of each drive to reduce the impedance to 20–100 kΩ after the VersaDrive was assembled. Ultrasonication (50 W, 40 kHz) was applied during the plating process to remove the weakly bonded plating and to create a stable impedance.

Stereotaxic surgery. In all stereotaxic surgeries, rats were anesthetized using isoflurane in air (1.5−3%), then fixed in a stereotaxic frame (ASI Instruments). Body temperature was maintained at 37°C with a heating pad during the surgery. Baytril (200 μl/kg; Bayer) and Metacam (200 μl/kg; Boehringer Ingelheim Vetmedica) were each diluted into 0.5 ml of saline and then injected subcutaneously at the end of the surgery. After surgery, rats were injected with antibiotic Baytril (50–100 μl/kg; Baytril) for 5 d and housed individually for at least 7 d with food and water provided *ad libitum*.

VersaDrive implantation. Stereotaxic surgery was conducted to implant two VersaDrives with two/four independently movable drives unilaterally into the mPFC and the CA1 region of the HPC or to implant one VersaDrive with eight independently movable drives unilaterally into the mPFC. The VersaDrives were implanted aiming at the following coordinates relative to bregma: mPFC: anteroposterior (AP), +3.2 to +4.2 mm; ML, +0.1 to +0.9 mm or +1.8 mm (with 18° angle); DV, −3.2 to −4.8 mm; HPC: AP, −5.4 to −6.2 mm; ML, +5.4 to +5.8 mm; DV, −3.7 to −3.8 mm. Coordinates of the HPC were targeted to a part of the HPC that is known to project to the mPFC (Jay and Witter, 1991; Verwer et al., 1997; Cenquizca and Swanson, 2007; Hoover and Vertes, 2007). The ground wires were placed beneath the skull and above the dura through a small hole drilled in the contralateral side of the skull. After animals recovered from surgery, the tetrodes were gradually lowered by turning the screws anticlockwise on the drive to reach a depth corresponding to the targeted brain regions. The tetrodes were advanced in 0.125 mm steps and tested for unit activity 6–8 h after each advancement until spontaneous neural activity was observed simultaneously on several tetrodes.

Viral constructs. AAV2/1 pSyn-ArchT-GFP [7.56×10^{13} viral genomes (vg)/ml], Retro-AAV pAM-EGFP (2.07×10^{12} vg/ml), and AAV DJ/8 pAM-tdTomato (2.81×10^{13} vg/ml) vectors were produced in-house at the University of Queensland. AAV5.hSyn-eYFP.WPRE (1.25×10^{13} vg/ml) was obtained from the University of Pennsylvania Vector Core (Philadelphia, PA).

Virus injection and optical fiber implantation. To map the HPC projection to the mPFC, retrogradely transported adeno-associated virus (AAV; Retro-AAV pAM-EGFP mixed with marker AAV DJ/8 pAM-tdTomato; 3:1 ratio; 0.4–0.6 μl) was unilaterally injected in the mPFC (right hemisphere), using the following coordinates relative to bregma: AP, + 3.0 mm; ML, + 0.4 mm; DV, – 4.3 mm. For terminal inhibition of the HPC → mPFC projection at the mPFC, bilateral viral delivery (AAV 2/1 pSyn-ArchT-GFP or AAV5.hSyn-eYFP.WPRE as the control; 0.4–0.6 μl on each side) into the CA1 region of the HPC was aimed at the following coordinates relative to bregma: AP, −5.80 mm; ML, +5.4 mm; DV, −3.9 mm. Optical fibers (core diameter, 200 μm; outer diameter, 240 μm; numerical aperture, 0.22; Doric Lenses) were bilaterally implanted into the mPFC aimed at the following coordinates relative to bregma: dual fiber-optic cannulas: AP, +3.0 mm; ML, ±0.5 mm; and DV, −4.4 mm; mono fiber-optic cannulas: AP, +3.0 mm; ML, ±2.8 mm (with 22° angle); and DV, −4.8 mm. Virus was injected via a 30 gauge needle attached to a 5 μl Hamilton syringe via plastic tubing (PlasticsOne). A microsyringe pump and its controller were used to control the speed of the injection (0.1–0.2 μl/min). The needles were slowly removed 5–10 min after injections. The incision in the scalp was sutured and sealed using Vetbond Tissue Adhesive (3M). Retrograde virus injection and projection sites were investigated 4 weeks after injection. Behavioral experiments investigating the HPC → mPFC projection were performed 4–5 weeks following viral injection.

Behavior. The NOR task was undertaken in a 60 cm (width) × 60 cm (length) × 45 cm (height) open field arena, constructed from dark plastic material. The objects included 375 ml aluminum coke cans, 400 ml glass beakers, ceramic coffee cups, rubber balls, rubber cubes, paper cups, and glass bottles of approximately the same height. Objects were placed in the center of the arena with a 20 cm center distance between them and a 20 cm center distance to the arena walls. The placement of the objects was counterbalanced by side and the order of object choice in different sessions was randomly assigned across animals. The arena and all the objects used were cleaned with 70% alcohol and distilled water between sessions.

For the electrophysiological study, the rats were exposed to the experimental apparatus in the absence of objects in two daily 10 min sessions that were separated by at least 2 h (habituation). They were then exposed to two identical sample objects, A1 and A2, for a 10 min session

(training). After a 24 h retention interval, animals were placed in the arena with one familiar object A and one novel object B, with 10 min of exploration (test 1). Twenty-four hours after test 1, the rats were again placed in the arena for 10 min with the same familiar object A but with a second, different novel object C, followed by further exploration of the novel object (test 2) and the acquisition of data. Thus, each rat was tested and recorded twice, with each of the recordings analyzed separately. We did two test sessions in the electrophysiological experiments to increase the yield of single units.

For the identical objects task experiment, the test procedure was varied so that rats were exposed to the same two identical objects (familiar objects) from training. For the nonidentical objects task experiment, the animals were exposed to two nonidentical objects after habituation to examine nonmnemonic aspects of object discrimination.

For the c-Fos study, the test procedure was varied so that animals were exposed either to a novel and a familiar object (NOR group) or to two familiar objects from training (control group). This adjustment was necessary to allow us to compare neuronal activity during exploration of a novel object versus familiar objects in separate animals following one test session. A 24 h retention delay for the NOR task was chosen, given that both the HPC and mPFC have been shown to be important for delay-dependent, long-term, rather than short-term, recognition memory (Akirav and Maroun, 2006; Clarke et al., 2010; Pezze et al., 2015).

Behavior was recorded by a digital camera (FlyCapture Flea 2) and the exploration behavior of the animals was first analyzed using EthoVision software (Noldus) and then corrected manually. Heat maps of the exploratory behavior were generated for the area surrounding the objects (15 cm) unless otherwise indicated. The exploration of objects was scored as the time the animal spent either facing an object (nose within 5 cm distance), or touching (face or forepaws), sniffing, or licking the object. The epochs of exploration were excluded for electrophysiological data analysis if the duration was <3 s or if there were significant artifacts, otherwise all were included. The resting state epochs were selected as at least 5 s periods in each session when the rat was not exploring any object or arena. At least three different resting epochs were chosen for one session per animal to obtain the averaged resting state neural activity. The range of the epochs number is from 3–15 depending on individual animals.

The object discrimination index was defined as the novel object exploration time of the animal minus the familiar object exploration time divided by the total exploration in the NOR test session. The NOR behavior index was defined as the novel object exploration time of the animal divided by the total exploration in the NOR test session.

In vivo recording. Implanted VersaDrives were connected to headstages (Axona) containing unity-gain operational amplifiers. Each headstage was connected to a 16-channel preamplifier and the recorded primary signals were digitized by the Analog-to-Digital Converter at a rate of 48 kHz. The digitized signal was then fed into the system unit, and the processing was divided into two categories to record local field potential (LFP; gain, 200×, 500× or 1000×; cutoff filter, 1 kHz; notch filter, 50 Hz) and single-unit activity (gain, 6000×; bandpass filter, 300–7000 Hz), respectively. At the conclusion of the experiment, recording sites were marked with electrolytic lesions before perfusion, and electrode tip locations were reconstructed with standard histologic techniques (see details in Immunohistochemistry section). Rats were excluded from LFP or single-unit data analysis if the electrode placement was outside the targeted brain regions.

Local field potential analysis. Raw LFP recording data were saved in binary format files and converted into .mat files in MATLAB (MathWorks) in microvolt units. LFP data were then clustered into canonical frequency bands (theta, 4–10 Hz; beta, 10–30 Hz; slow gamma, 30–55 Hz; fast gamma, 55–100 Hz) using a discrete-form finite impulse response bandpass filter. The attenuation in the stop band was set as 80 dB, and the amount of ripple allowed in the pass band was 1 dB. The frequency differences between the start of the first stop band and the start of the first pass band, and between the start of the second pass band and the start of the second stop band were both 0.5 Hz.

Hilbert transform was used to obtain the instantaneous amplitude $a(t)$ and instantaneous phase $\varphi(t)$ of the signal at every time point, shown as $a(t)e^{-i\varphi(t)}$. The averaged LFP amplitude A_{state} in different behavioral states (i.e., resting state, familiar object exploration, and novel object exploration) was retrieved by averaging the instantaneous amplitude of the filtered LFP in particular behavioral epochs $(e_1, e_2 \ldots e_n)$ of the corresponding behavioral state, as follows:

$$A_{\text{state}} = \frac{\overline{A(e_1)} + \overline{A(e_2)} + \ldots + \overline{A(e_n)}}{n}.$$

The LFP NOR index was defined as the mean LFP activity during novel object exploration divided by the sum of the mean LFP activity during the familiar and novel object exploration in the NOR test session.

To determine the functional connectivity (neural coupling) between two brain regions, cross-correlation analysis was performed in MATLAB (xcorr function). The instantaneous amplitudes of the recorded LFPs from the mPFC and the HPC were considered as two discrete-time sequences $x(n)$ and $y(n)$, respectively. The cross-correlation coefficient $\hat{R}_{xy,\text{coeff}}$ was calculated by the xcorr function in MATLAB as the following formula (the asterisk denotes complex conjugation):

$$\hat{R}_{xy}(m) = \begin{cases} \sum_{n=0}^{N-m-1} x_{n+m} y_n^*, m \geq 0, \\ \hat{R}^*_{yx}(-m), m<0 \end{cases}$$

$$\hat{R}_{xy,\text{coeff}}(m) = \frac{1}{\sqrt{\hat{R}_{xx}(0)\hat{R}_{yy}(0)}} \hat{R}_{xy}(m).$$

The averaged peak cross-correlation coefficient C_{state} in different behavioral states (i.e., resting state, familiar object exploration and novel object exploration) was retrieved by averaging the peak cross-correlation coefficient $\hat{R}_{xy,\text{coeff}}$ in particular behavioral epochs $(e_1, e_2 \ldots e_n)$ of the corresponding behavioral state, as follows:

$$C_{\text{state}} = \frac{\overline{C(e_1)} + \overline{C(e_2)} + \ldots + \overline{C(e_n)}}{n}.$$

The LFP coupling NOR index was defined as the mean peak correlation coefficient during novel object exploration divided by the sum of the mean peak correlation coefficient during the familiar and novel object exploration in the NOR test session.

Hilbert transform was used to calculate the instantaneous phase $\varphi(t)$ of the simultaneously recorded mPFC and HPC signals at each time point. The phase difference was calculated as the subtraction of the mPFC signal phase of the corresponding HPC signal phase of the time point: $\Delta\varphi(t_n) = \varphi_{\text{HPC}}(t_n) - \varphi_{\text{mPFC}}(t_n)$. The phase differences of each time point between the two regions were acquired, and the results were plotted in a histogram to display the probability distribution. The mean phase difference during NOR was calculated by averaging the HPC–mPFC phase differences across all the NOR epochs. The time lag from the HPC to the mPFC was calculated using 4–10 Hz theta temporal cycle (100–250 ms) times the mean phase difference divided by 360°.

To assess the causal interaction and directionality between the theta oscillations recorded in the two brain regions, spectrally resolved Granger causality was calculated for the LFP signals of the mPFC and the HPC. The application principle of Granger causality in this study considers the LFP signals from the mPFC and the HPC as temporal dynamics of two time series, $p(t)$ and $h(t)$; $h(t)$ causes $p(t)$ if the inclusion of past observations of $h(t)$ reduces the prediction error of $p(t)$ in a linear regression model of $p(t)$ and $h(t)$, compared with a model that includes only previous observations of $p(t)$. For these analyses, the MVGC multivariate Granger causality MATLAB toolbox (Barnett and Seth, 2014) was used to fit a higher-order vector autoregressive model to the processes. Model order was determined using the Bayesian information criterion. Frequency-domain multivariate G-causality of the HPC → mPFC

and the mPFC → HPC directionality was calculated in different behavioral states across animals. The 4–10 Hz (theta LFP) integral of the distribution curve was calculated in different behavioral states for statistical comparison.

For all the LFP analysis in the NOR test, we averaged the values between two NOR test sessions from one animal to get the mean as the final result for that animal in the test session unless otherwise indicated.

Single-unit clustering and analysis. Spike sorting was performed using Wave_Clus (Quiroga et al., 2004). Spikes were detected using an amplitude threshold which was derived from six times the SD of the baseline noise median (SNR >6). Feature vectors were then extracted from the spike waveforms using wavelet transform to extract the wavelet coefficients, with each coefficient characterizing the spike shapes at different scales and times. The first 10 coefficients with the largest deviation from normality were selected based on a modified Kolmogorov–Smirnov test (Press, 1992) and served as the input to the clustering algorithm. The wavelet coefficients were then clustered using superparamagnetic clustering, which is based on simulated interactions between each data point and its K-nearest neighbors (Blatt et al., 1996). A group of waveforms was considered to be generated from a single neuron if the waveforms formed a discrete, isolated cluster in the wavelet space (by visual inspection). To separate clusters reliably, we also tested the autocorrelograms of each cluster, which had to show a refractory period ≥2 ms for >98% of spike events. To achieve a better yield of unit data, tetrodes were advanced at least 0.250 mm between the NOR test 1 and test 2 sessions to ensure that different units were recorded in the two test sessions. If the tetrodes were still within the mPFC region after one cycle of the NOR protocol, this protocol was repeated with a completely different set of objects in a second cycle.

Cell responsiveness was assessed with respect to behavioral state-evoked activity (first 3 s after the behavioral state onset, which was defined as a trial) and behavioral state-related changes in firing rates. In the case of behavioral state-evoked activity, a cell was considered responsive if it increased or decreased its firing rate in response to the behavioral state. To assess the statistical significance of unit behavioral state responses, we compared the firing rates during the time bins in the first 3 s following behavioral state onset to the 3 s preonset baseline (100 ms bins) using rank-sum tests with a significance threshold of $p < 0.01$.

The mean firing rate of a neuron was calculated as the number of spikes in the recording duration divided by the duration of the recording. We divided neurons into the following two groups: putative principal neurons (PNs) with a mean firing rate <3 Hz, and putative interneurons (INs) with a mean firing rate >3 Hz (see Fig. 5*D*). To assess differences in the characteristics of PNs and INs, we compared the burst statistics and half spike width for PNs, and INs pooled across all rats. The burst statistics was measured by interspike interval (ISI) coefficient (Tattersall et al., 2014) for a given spike train. An ISI histogram was generated (bin size, 1 ms; lag, 100 ms), and the ISI coefficient (burst index) was calculated as the SD of the ISI divided by the mean ISI. A higher value of ISI coefficient (burst index) indicates more bursting. The half-spike width of each neuron was calculated as the width of the average spike waveform at half-maximal amplitude. To evaluate the correlated activity of pairs of neurons, we calculated the cross-correlogram of the spike train for each neuron with 0.5 ms bins, at up to 20 ms lag. This equated to shifting the spike train of one neuron relative to the other spike train by between −20 and 20 ms, at 0.5 ms intervals, and calculating the correlation between the spike trains at each step.

Optogenetic inhibition. To silence HPC input onto the mPFC, AAV2/1 pSyn-ArchT-GFP virus was injected into the CA1 region of the HPC. Control animals received AAV5.hSyn-eYFP.WPRE at the same target. The rats went through the same NOR protocol as described above. During the NOR test sessions (10 min), rats received five cycles of 1 min optical terminal inhibition in the mPFC (561 nm laser; each hemisphere, 4–6 mW; constant; Laserglow Technologies) with a 1 min light-off interval.

Immunohistochemistry. Rats with electrode implantation were killed with a lethal dose of isoflurane following behavioral procedures. Electrolytic lesions to mark the tips of the tetrode were generated by a 70 μA direct current for 5 s. The animals were then perfused through the left ventricle with 4% paraformaldehyde (PFA) in 1× PBS. Brains were dissected from the skull and fixed in PFA for 24 h at 4°C. They then were sliced into 100 μm coronal sections using a vibratome (VT1000S vibrating blade microtome, Leica Biosystems). Sliced tissue sections were stained with 4′,6′-diamidino-2-phenylindole dihydrochloride (DAPI; 1 μg/ml; Sigma-Aldrich) for 5 min at room temperature, then washed in PBS three times. The sections were mounted on microscope slides and coated with antifade solution and a glass coverslip. Electrolytic lesions were identified and verified with an upright fluorescence microscope (Axio Imager/Observer, Zeiss), and images were taken with a 5× objective using both a DAPI fluorescence filter and bright-field imaging. The perfusion, slicing, and DAPI staining procedures for animals with virus injection were the same as those for the electrode-implanted animals. Slices were imaged with an upright fluorescence microscope (5× or 20×; Axio Imager/Observer, Zeiss) or a confocal system (20×; LSM510, Zeiss).

Rats contributing to the c-Fos study were anesthetized (pentobarbitone, 120 mg/kg) 2 h after commencement of the NOR test and transcardially perfused as described above. Brains were postfixed (30 min) and cryoprotected in 20% sucrose (48 h) before sectioning on a cryostat (40 μm thick and collected every 160 μm; Lecia Biosystems). Sections were stored at 4°C in 0.1% sodium azide in phosphate buffer (PB) until use. For immunohistochemistry procedures (Furlong et al., 2016), sections were prepared in 50% ethanol, 50% ethanol with 3% hydrogen peroxide, and 5% horse serum in PB (30 min each) before incubation in rabbit anti-c-Fos antibody (1:1000; catalog #ABE457, Millipore) in 0.2% Triton X and 2% horse serum (48 h at room temperature). Sections were then rinsed in PB and incubated in donkey anti-rabbit secondary antibody (for 12 h; 1:1000; catalog #711–065-152, Jackson ImmunoResearch) followed by avidin–biotin complex reagent (for 3 h; 1:200; Vectastain Elite, Vector Laboratories). For the nickel-intensified diaminobenzidine (DAB) reaction, sections were first incubated in a solution of 0.5% DAB, 0.04% ammonium chloride, 0.2% D-glucose, and 1% nickel sulfate in sodium acetate buffer, pH 6 (for 10 min), after which glucose oxidase was added (for 10 min; 735 U/ml; Sigma-Aldrich). Finally, sections were mounted on gelatin-coated slides, coverslipped with Entellan, and scanned using an Aperio Scanscope slide scanner (20× objective; Leica Biosystems). Fos in the CA1 region of the HPC and mPFC was quantified using the thresholding tool in ImageJ software (National Institutes of Health) by an experimenter blind to group. The sections that were quantified corresponded with the site of *in vivo* electrophysiological recordings and were selected based on landmarks from the atlas of Paxinos and Watson (2007). For HPC, three sections were chosen between bregma −5.4 and −5.88 mm, and the entire CA1 region was quantified dorsoventrally based on the visible pyramidal cell layer. For the mPFC, three sections were chosen between bregma 3.72 and 3.00 mm, and the mPFC was quantified between the top border of forceps minor (of corpus collosum) and the bottom border of the claustrum. The number of Fos-positive cells for each region were calculated by averaging the counts of the three sections divided by the size of the area quantified in square millimeters, as determined using the measuring tool in ImageJ.

Statistical analysis. GraphPad Prism version 8.0 and MATLAB were used for statistical analysis. No statistical methods were used to predetermine sample size. Normal distribution was tested in all the dataset using the Kolmogorov–Smirnov test: if the dataset passed the normality test, parametric tests were used. Otherwise, nonparametric tests were used. Outliers were determined using a Grubb's test. Two-group comparisons were assessed using two-sided paired or unpaired *t* test (parametric tests), or two-sided Wilcoxon matched-pairs signed-rank test or Mann–Whitney test (nonparametric tests). Multiple-group comparisons were assessed using one-way ANOVA test with repeated measures followed by a *post hoc* Tukey's multiple-comparison test (parametric test) to identify significant groups as indicated in the figure legend, or a Friedman test with repeated measures followed by a *post hoc* Dunn's multiple-comparison test (nonparametric test) to identify significant groups, as indicated in the figure legend. The archaerhodopsin (ArchT)/enhanced yellow fluorescent protein (eYFP) injection and laser stimulation were used as two main factors for the two-way ANOVA. The ArchT/eYFP

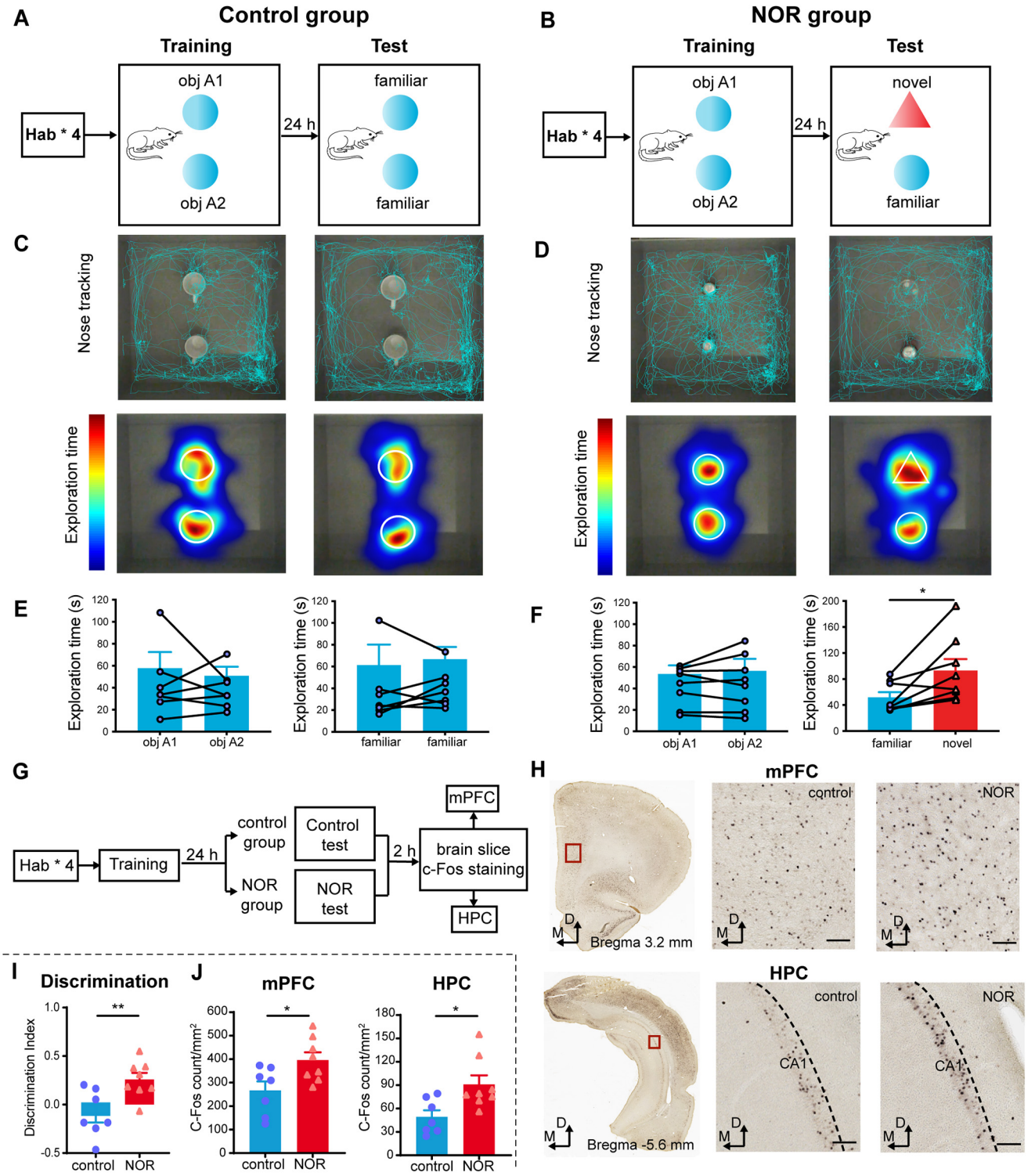

Figure 1. c-Fos expression increases in the mPFC and HPC with NOR. ***A***, ***B***, Schematics illustrating the behavioral task for the control group (***A***) and the NOR group (***B***). ***C***, ***D***, Nose tracking (top) and exploratory behavior heat maps (bottom) of one representative rat during training (left) and test (right) in the control group (***C***) and the NOR group (***D***). ***E***, Rats in the control group showed no discrimination of the two identical objects in training (left; paired two-sided *t* test, $t_{(6)} = 0.4907$, $p > 0.05$, $N = 7$ rats) and testing (right; two-sided Wilcoxon matched-pairs signed-rank test, $p > 0.05$, $N = 7$ rats). Mean ± SEM. ***F***, Rats in the NOR group showed no discrimination of the two identical objects in training (left) but displayed novel object exploration preference in testing (right; two-sided Wilcoxon matched-pairs signed-rank test, $^*p < 0.05$, $N = 8$ rats). Values are the mean ± SEM. ***G***, Two experimental groups designed to examine NOR-related c-Fos expression. ***H***, Representative immunohistochemical staining for the c-Fos-positive cells from the control group and NOR group in the mPFC (top) and HPC (bottom). Scale bar, 100 μm. ***I***, The discrimination index between the NOR group and the control group (unpaired two-sided *t* test, control vs NOR, $t_{(13)} = 3.174$, $^{**}p < 0.01$). ***J***, Mean number of c-Fos-positive cells in the mPFC (left) and HPC (right) of the control and NOR groups (two-sided Mann–Whitney test; mPFC: Mann–Whitney $U = 7$, $^*p < 0.05$, $N = 7$ rats; unpaired two-sided *t* test: HPC: $t_{(13)} = 2.787$, $^*p < 0.05$, $N = 8$ rats). Values are the mean ± SEM.

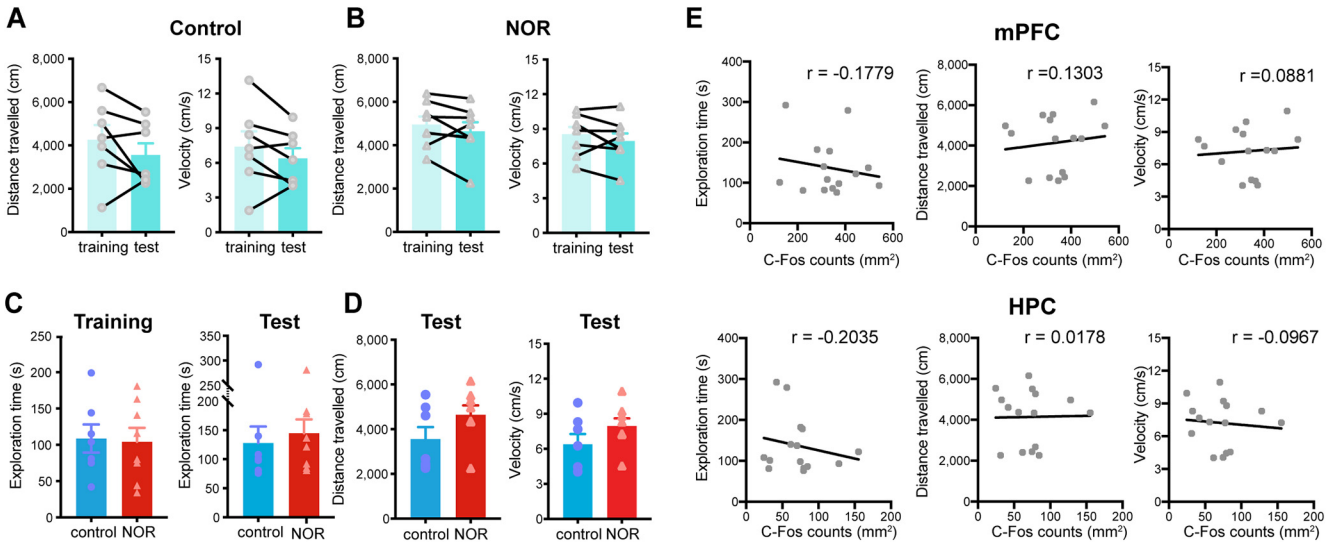

Figure 2. There is no change in overall locomotion during novel object exploration. ***A***, ***B***, Mean distance traveled (left) and velocity (right) during the training and test sessions for the rats in the control group (two-sided Wilcoxon matched-pairs signed-rank test, travel distance: $p > 0.05$; paired two-sided t test, velocity: $t_{(6)} = 1.455$, $p > 0.05$, $N = 7$ rats; ***A***) and NOR group (paired two-sided t test; travel distance: $t_{(7)} = 1.309$, $p > 0.05$; velocity: $t_{(7)} = 1.336$, $p > 0.05$, $N = 8$ rats; ***B***). Values are the mean ± SEM. ***C***, Mean total object exploration time between the control and NOR groups in the training (left) or test (right) session (unpaired two-sided t test, training: $t_{(13)} = 0.1573$, $p > 0.05$, $N = 7$ rats; two-sided Mann–Whitney test, test: Mann–Whitney $U = 22$, $p > 0.05$, $N = 8$ rats). Values are the mean ± SEM. ***D***, Mean distance traveled (left) and velocity (right) in the test session did not show change between the control and NOR groups (two-sided Mann–Whitney test, distance traveled: Mann–Whitney $U = 19$, $p > 0.05$, $N = 7$ rats; unpaired two-sided t test, velocity: $t_{(13)} = 1.437$, $p > 0.05$, $N = 8$ rats). Values are the mean ± SEM. ***E***, Correlation between the exploration time (left; $r = -0.1779$, $p > 0.05$), distance traveled (middle; $r = 0.1303$, $p > 0.05$), and velocity (right; $r = 0.0881$, $p > 0.05$) of individual rats and their mPFC c-Fos counts (top: $N = 15$ rats, two-sided Spearman's correlation test) or HPC c-Fos counts ($r = -0.2035$, $p > 0.05$, $r = -0.0178$, $p > 0.05$, $r = -0.0967$, $p > 0.05$; bottom: $N = 15$ rats, two-sided Spearman's correlation test).

injection, laser stimulation, and familiar/novel object exploration were used as three main factors for the three-way ANOVA. Multiple-variate comparisons were assessed using two-way ANOVA or three-way ANOVA with repeated measures, followed by a *post hoc* Bonferroni's multiple-comparison test to identify significant groups, as indicated in the figure legend. The analysis of the phase difference distribution uniformity was done using the Rayleigh's test. The analysis of the object responses of a unit was done using the rank-sum test. The analysis of the correlation between animal NOR behavior and c-Fos counts, theta LFP amplitude change and theta coupling change were done using the two-sided Pearson's correlation (parametric test) or Spearman's correlation (nonparametric test). The null hypothesis was rejected at the $p < 0.05$ level (except for the rank-sum test, which used a significance threshold of $p < 0.01$).

Results

To assess novelty discrimination, rats were placed in a 60 × 60 cm arena and first habituated to the context in four sessions over 2 d (see Materials and Methods). During the training phase, two identical, previously unseen objects were presented in the same arena. Twenty-four hours later, during the test session, rats were returned with either the same two (now familiar) objects in the same locations (Fig. 1*A*) or one object being replaced by a novel one (Fig. 1*B*). Consistent with previous reports (Ennaceur and Delacour, 1988), rats explored both objects for a similar amount of time during training, without significant object or location preference (Fig. 1*C–F*, left panels). However, during the test session, rats showed an exploration preference for the novel compared with the familiar object (Fig. 1*C–F*, right panels). There was a significant change in the discrimination index of the animal between the NOR and control groups (Fig. 1*I*), showing that they were able to recall memory of the previously experienced object and recognize the presence of a novel object.

To confirm the engagement of the HPC and mPFC in NOR, we first tested expression of the immediate early gene c-Fos (Fig. 1*G*), a marker for active cells (Herrera and Robertson, 1996). The presence of a novel object significantly enhanced c-Fos expression in the HPC and mPFC (Fig. 1*H*,*J*), showing that more neurons are engaged during exploration of a novel object. This enhancement was not because of the total time spent exploring the objects, differences in distance traveled, or velocity of movement, as these variables did not differ between the two groups or correlate with c-Fos expression in individual animals during test (Fig. 2). No significant correlation was found between the discrimination index and c-Fos expression in HPC or mPFC (data not shown; Pearson's correlation test: HPC: $r = 0.2845$, $p > 0.05$; mPFC: $r = -0.0959$, $p > 0.05$).

Theta activity in the mPFC and HPC is enhanced in NOR

The increase in c-Fos expression in the HPC and mPFC during NOR is consistent with findings that these two regions are part of the network of brain structures that contribute to NOR (Barbosa et al., 2013; Tanimizu et al., 2018). To test whether neural activity in these two regions correlates with NOR behavior, simultaneous LFP recordings were obtained from the mPFC and HPC (Fig. 3*A*). Region-specific LFP oscillations provide an indicator of the network activity associated with particular behavioral states (Buzsáki, 2006; Buzsáki et al., 2012). Animals with implanted electrodes underwent the same behavioral program as in Figure 1 with slight modification: all animals were first habituated to the context in four sessions over 2 d, followed by a single training session in which two identical objects were placed in the habituation context. The next day, they were returned to the same context, with one object replaced by a novel one. In a second test session 24 h later, the familiar object was retained, but a second novel object was introduced into the same location. In both test sessions, animals showed a significant preference for the novel object with no change in the discrimination index, total distance traveled or velocity (data not shown).

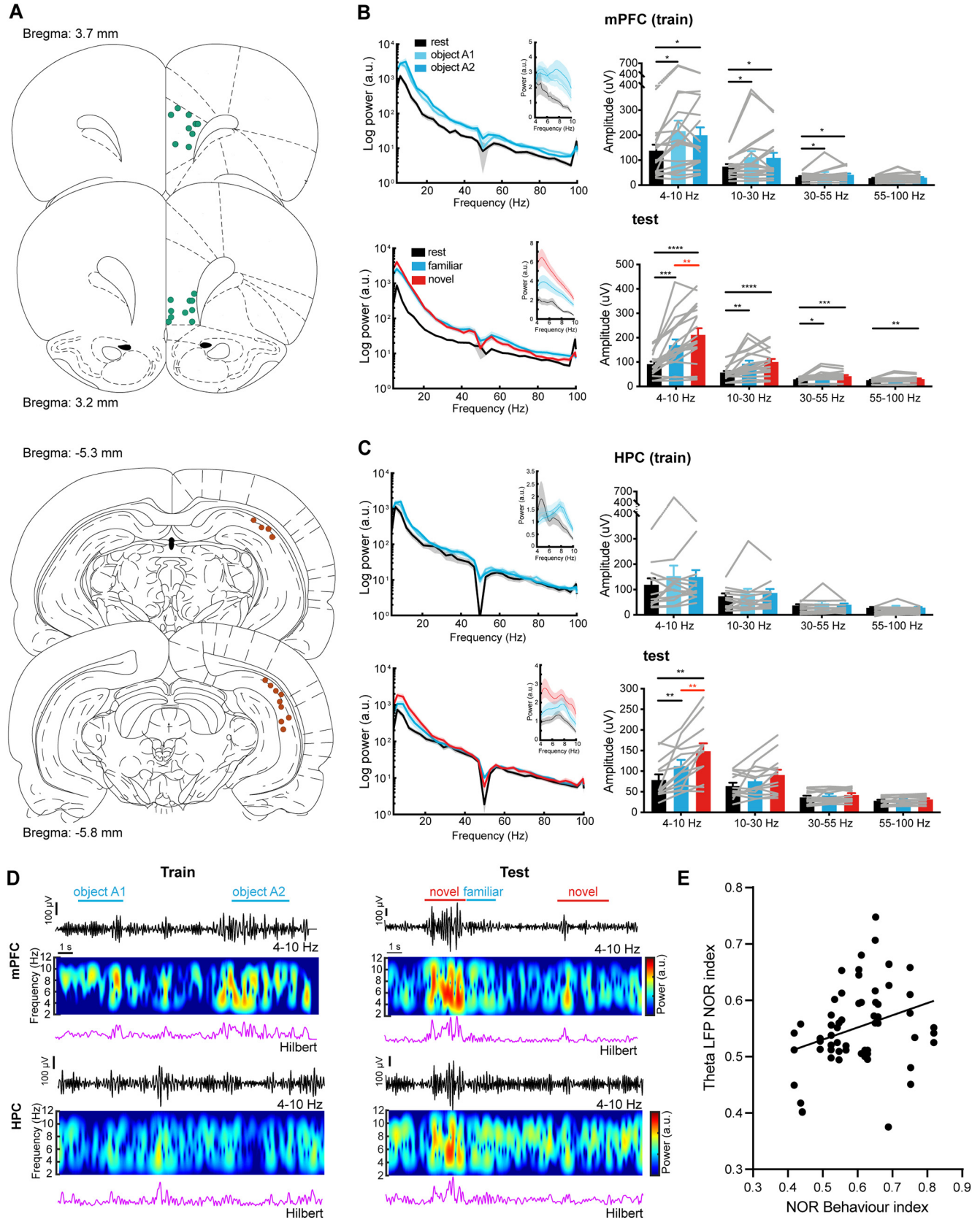

Figure 3. Novel object recognition enhances theta (4–10 Hz) activity in the mPFC and HPC. ***A***, Schematics showing the placement of LFP recording electrode tips in the mPFC (top, $n = 19$) and the HPC (bottom, $n = 13$). Bregma locations for each section are indicated. ***B***, Left, Mean log PSD in the mPFC during resting state, and object exploration during training (top) and testing (bottom). Insets show the mean PSD within 4–10 Hz. Right, Mean LFP amplitudes from the mPFC for different frequency bands are shown during training (top) and testing (bottom; Friedman test with repeated measures: mPFC training, $n = 19$; theta, Friedman statistic = 9.680; beta, Friedman statistic = 9.579; slow gamma, Friedman statistic = 10.96; fast gamma, Friedman statistic = 6.836. mPFC test, $n = 19$. One-way ANOVA with repeated measures: theta, $F_{(2,16)} = 26.77$; Friedman test with repeated measures: beta, Friedman statistic = 21.89; slow gamma,

LFP recordings in mPFC and HPC were obtained during both training and test sessions. The LFP power spectral density (PSD) amplitude was separated into the following four frequency ranges: theta (4–10 Hz), beta (10–30 Hz), slow gamma (30–55 Hz), and fast gamma (55–100 Hz). During training, both objects are novel and led to significant increases in theta-, beta-, and slow gamma-band activity in the mPFC during exploration of either of the two objects, compared with the resting state, with no difference between the two objects (Fig. 3*B*, top, *D*, left top). In contrast, there was no significant change in HPC activity during training (Fig. 3*C*, top, *D*, left bottom). However, during the test session, LFP activity was enhanced in both the mPFC and HPC (Fig. 3*B*,*C*, bottom, *D*, right) during NOR compared with the resting state and familiar object exploration. Importantly, the increase of LFP power during novel object exploration (compared with familiar object exploration) was restricted to the theta band and was correlated with the NOR behavior of the animals across all the test sessions (Fig. 3*E*), supporting a role for the mPFC and HPC in NOR. The fact that there was no significant change in LFP power in the HPC during the training session provides a valuable internal control for the NOR-related theta activity, showing that the LFP activity change was not merely caused by motor behaviors during object exploration.

HPC–mPFC theta coupling is enhanced in NOR and driven by the HPC

Temporally coupled oscillatory activity between brain areas facilitates interregional communication (Buzsáki and Draguhn, 2004), and previous studies have identified an increase in synchronized activity between the HPC and mPFC during spatial memory tasks (Jones and Wilson, 2005; Abbas et al., 2018). We have shown that theta oscillations are enhanced in the mPFC and HPC during novel object recognition (Fig. 3*B*–*D*), and simultaneous recordings suggest that the increase in theta are time locked (Fig. 3*D*, right). We therefore tested whether oscillations in these two regions were temporally coupled. Cross-correlation analysis of the LFP between the HPC and mPFC during training showed no significant change in theta band coupling during exploration of either object compared with the resting state (Fig. 4*A*), whereas in the test session HPC–mPFC-coupled theta activity was enhanced during the exploration of both novel and familiar objects (Fig. 4*B*). Moreover, there was a significant increase from the familiar to novel object exploration (Fig. 4*B*, right), and this enhanced theta coupling correlated with the NOR behavior of the animal (Fig. 4*C*), suggesting that recognition memory-guided behavior is mediated by an increase in temporally coupled HPC–mPFC theta activity.

To determine whether the enhanced theta coupling is driven by the mPFC or HPC, we evaluated the phase difference between theta LFPs in these two regions during NOR. This analysis revealed that the phase difference between the HPC and mPFC theta bands across all NOR epochs formed a unimodal distribution (Fig. 4*D*) with a positive skewness (median, 20.8°; time lag, 6–14 ms). This analysis shows that during NOR, theta activity in the HPC leads that in the mPFC. As an independent verification of this result, we calculated the Granger causality index (Barnett and Seth, 2014) to determine potential causal influences between the mPFC and HPC. No clear driven causality in either direction was observed in any behavioral state during training (data not shown), or during rest or familiar object exploration in the test session (Fig. 4*E*, left, middle). However, there was a strong theta-driven causality from the HPC to the mPFC during NOR (Fig. 4*E*, right), again supporting the notion that the HPC drives the mPFC during NOR through theta coupling. In agreement with this proposal, and consistent with previous anatomic studies (Hoover and Vertes, 2007), injection of retrogradely transported AAV-retro-pAM-EGFP into the mPFC (Fig. 4*F*) revealed extensive labeling of neurons in the same areas of the HPC CA1 region as our recording electrodes, showing monosynaptic synaptic connectivity between these regions (Fig. 4*G*).

Principal neurons and interneurons in the mPFC respond differently during object recognition

We have shown that during NOR, there is enhanced theta coupling between the HPC and mPFC, likely driven by direct HPC projections to the mPFC. To understand the changes in neural firing in the mPFC during NOR, we isolated single-unit activity in the mPFC during object recognition using tetrodes (Fig. 5). Recordings were obtained from nine implanted animals (Fig. 5*H*) with 42 units isolated during the training session, and 84 units during the test session. Neurons were classified as putative PNs or INs, with interneurons having a significantly higher basal discharge rate (>3 Hz) and a lower probability of burst firing (Csicsvari et al., 1998; Fig. 5*D*,*E*). Cross-correlogram analysis confirmed that neurons classified as INs inhibited the discharge of local neurons, whereas neurons classified as PNs excited them (Fig. 5*G*). Overall, in the training session, 21% of the sorted neurons were classified as INs (9 of 42), and 29% (24 of 84) were classified during testing (Fig. 5*F*).

To quantify the response of individual mPFC units, we compared the firing rates in 3 s time bins before and during the object exploration epoch (defined as a "trial" in this analysis). This analysis revealed that during object exploration there was an increase in discharge in some neurons in the mPFC (Fig. 6*A1*, *A2*), there was a decrease in others (Fig. 6*B1*,*B2*), and no response in many (Fig. 6*C1*,*C2*). Overall, during object exploration, 11 of 42 units (26%) responded during the training session (Fig. 6*D*, top). Of these, nine units were classified as PNs, of which seven (78%) increased their discharge but two (22%) were inhibited (examples are shown in Movies 1, 2). Only two of the responsive cells were INs and both (100%) reduced their discharge rate during object exploration (Fig. 6*E*). During the test session, 27 of 84 neurons (32%) responded as follows during object exploration: 9 to the familiar object; 10 to the novel object; and 8 to both (Fig. 6*D*, bottom). Exploration of the familiar object increased the discharge in 7 of 17 units (41%; 5 INs, 2 PNs), while 10 of 17 units (59%) were inhibited (3 INs, 7 PNs). The majority of the novel object-responsive PNs decreased their

←

Friedman statistic = 15.81; fast gamma, Friedman statistic = 11.53). ***C***, Left, Mean log PSD in the HPC during resting state, and object exploration during training (top) and testing (bottom). Insets show the mean PSD within 4–10 Hz. Right, Mean amplitudes from the HPC LFP for different frequency bands are shown during training (top) and testing (bottom; Friedman test with repeated measures: HPC training, $n = 13$; theta, Friedman statistic = 5.692; beta: Friedman statistic = 0.4615; slow gamma, Friedman statistic = 3.447; fast gamma: Friedman statistic = 2.851. One-way ANOVA with repeated measures; HPC test, $n = 13$; theta, $F_{(2,10)} = 17.15$; beta: $F_{(2,10)} = 4.955$; slow gamma: $F_{(2,10)} = 2.661$; fast gamma: $F_{(2,10)} = 3.218$). Values are the mean ± SEM. *n* represents the number of LFP recording sites. $^{*}p < 0.05$, $^{**}p < 0.01$, $^{***}p < 0.001$, $^{****}p < 0.0001$. ***D***, Representative example of simultaneous recordings from mPFC (top) and HPC (bottom). Traces on top show the filtered (4–10 Hz) LFP, color-coded PSD (middle), and Hilbert amplitude (bottom) during the training session (left) and the test session (right). Specific object exploration epochs are indicated by the colored lines. ***E***, Correlation between the mPFC/HPC theta LFP NOR index and the NOR behavior index of the animals ($r = 0.3046$, $^{*}p < 0.05$, $n = 61$ sessions, two-sided Pearson's correlation).

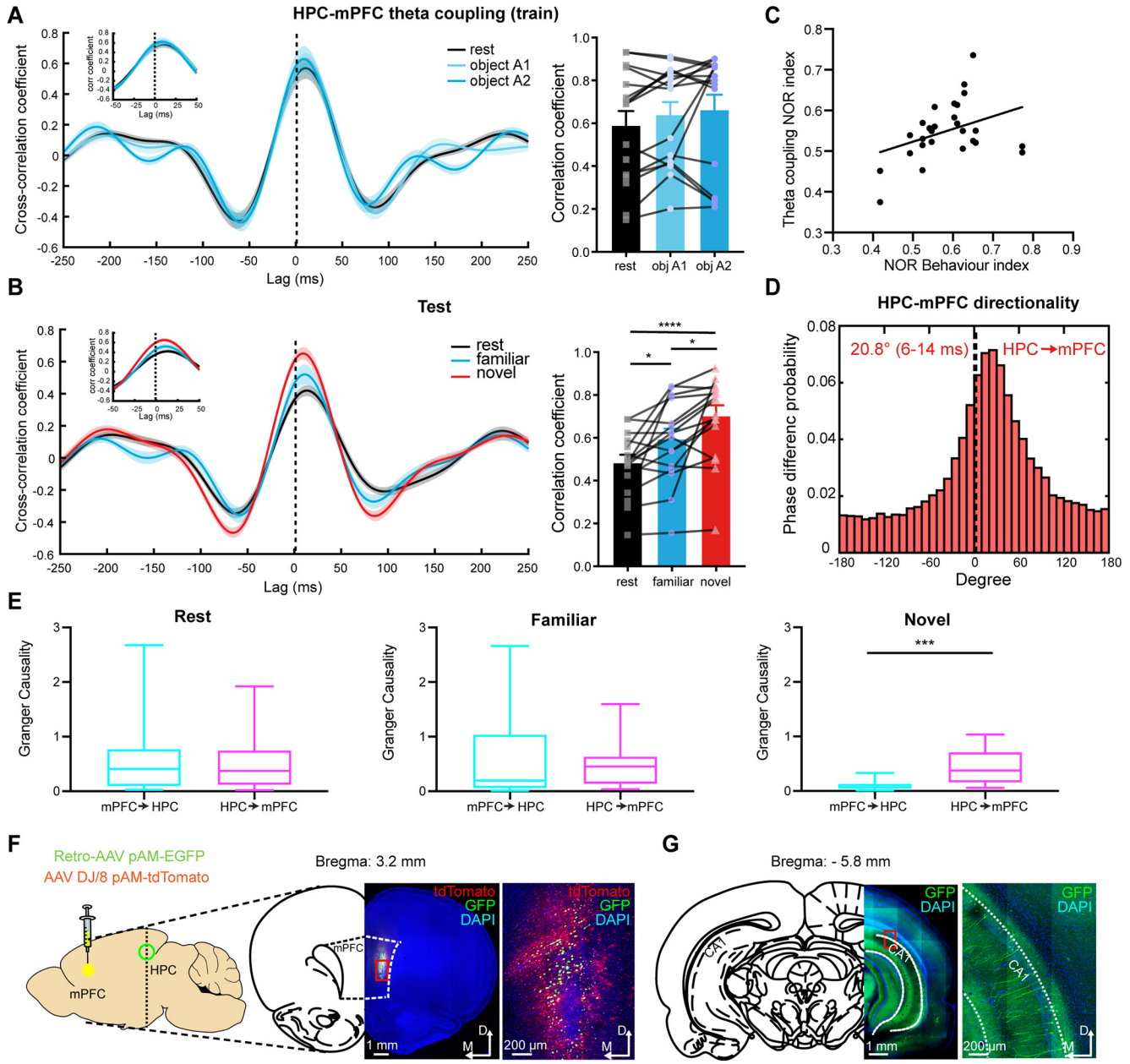

Figure 4. HPC–mPFC theta (4–10 Hz) coupling is enhanced during NOR. ***A***, Left, The HPC–mPFC theta LFP cross-correlation during training. Right, Mean peak HPC–mPFC theta LFPs cross-correlation coefficient showed no significant difference in NOR training (Friedman test with repeated measures; Friedman statistic = 1.556, $n = 16$ LFP pairs). Values are the mean ± SEM. ***B***, Left, The HPC–mPFC theta LFP cross-correlation during test. Right, The mean peak HPC–mPFC theta LFP cross-correlation coefficient showed significant enhancement in the NOR test (one-way ANOVA with repeated measures: $F_{(2,13)} = 12.77$, $n = 16$ LFP pairs). The dashed line represents the zero-lag time. Values are the mean ± SEM. *$p < 0.05$, ****$p < 0.0001$. The insets show correlation within ±50 ms. ***C***, Correlation between the mPFC/HPC theta LFP coupling NOR index and the NOR behavioral index (two-sided Pearson's correlation: $r = 0.3046$, $p < 0.05$, $n = 28$ sessions). ***D***, Phase difference probability histograms of the HPC–mPFC theta LFPs during NOR (Rayleigh's test, $p < 0.0001$; bin size = 10°). ***E***, Theta spectral Granger causality of the HPC driving the mPFC (magenta, HPC → mPFC) and the mPFC driving the HPC (cyan, mPFC → HPC) in the NOR test session (two-sided Wilcoxon matched-pairs signed-rank test: ***$p < 0.001$, $n = 16$ LFP pairs). In the box plots, the boundary of the box closest to zero indicates the 25th percentile, a line within the box marks the median, and the boundary of the box farthest from zero indicates the 75th percentile. Whiskers above and below the box indicate the maximum and minimum. ***F***, Unilateral injection of retrogradely transported AAV (GFP) into the rat mPFC (AAV DJ/8 vector was used as a marker: tdTomato). ***G***, Labeled pyramidal neurons in the ipsilateral CA1 region of the ventral HPC.

firing (61%, 9 of 13 units), whereas 60% (3 of 5 units) of the novel object-responsive INs increased their firing (Fig. 6*F*). Together, these results show that during training, PNs in the mPFC tend to increase their firing rate during object exploration (Fig. 6*E*), while in the test session they are more likely to be inhibited. By contrast, INs showed a trend toward increased firing to both the familiar and novel objects during the test session (Fig. 6*F*).

To test the response of mPFC neurons to previously encountered objects without novelty, a separate group of rats was tested with the same two objects that were presented in the training session (Fig. 6*G*). As seen in the prior NOR paradigm, 9 of 36 units (25%) responded during object exploration in the training session (Fig. 6*H*, left), and the majority of the object-responsive PNs (5 of 7 units) increased their discharge (71%; Fig. 6*I*, left). However, in the test session, only 4 of 30 units (13%; Fig. 6*H*, right) responded to the two identical (familiar) objects during object exploration, many fewer than the 32% in the NOR

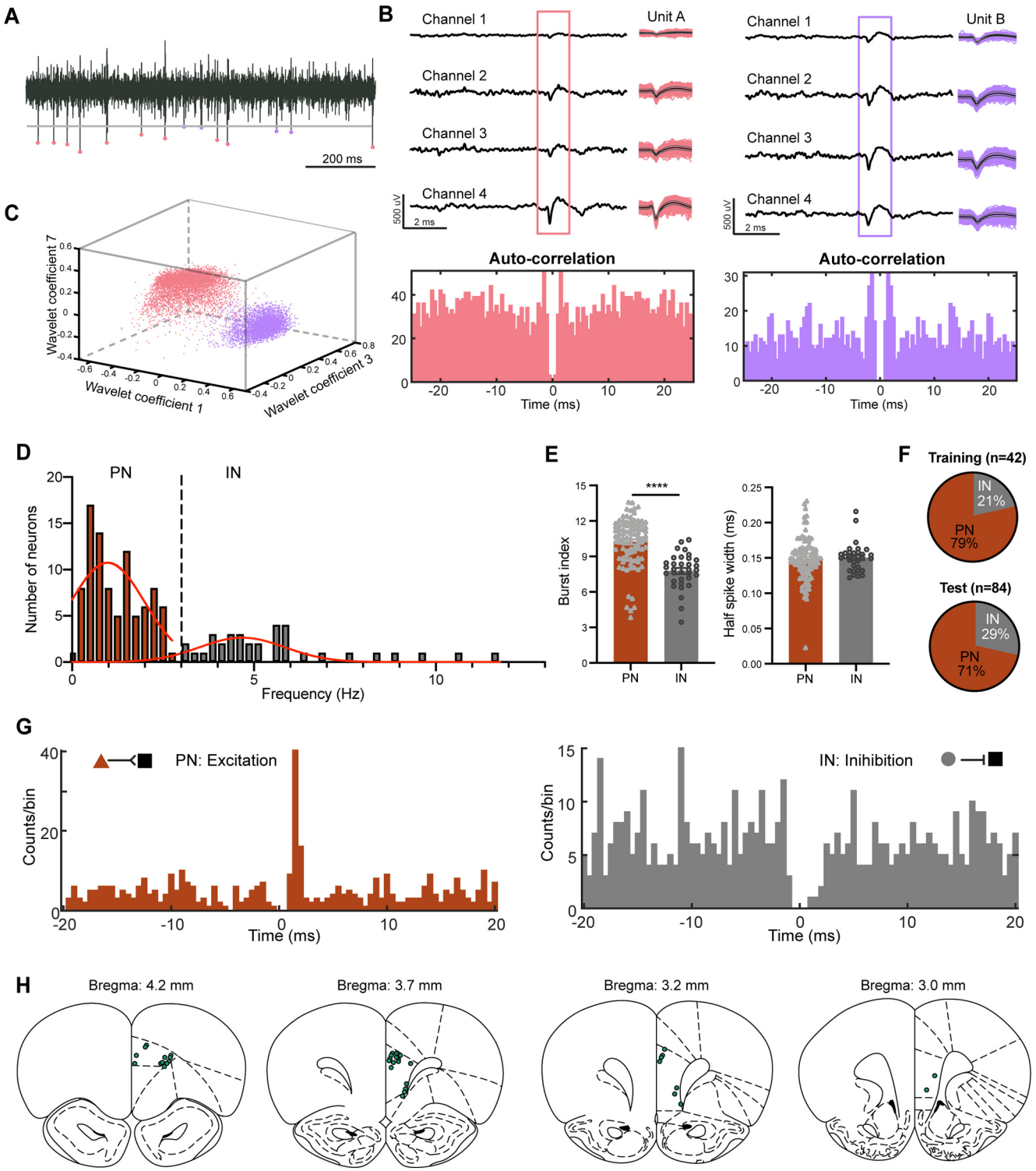

Figure 5. Principal neurons and interneurons in the mPFC during the NOR task. ***A***, Raw trace showing extracellular unit activity recorded from the mPFC. Two distinct units from one tetrode in the mPFC during one test session, marked by different colors. Unit A, Rose; Unit B, lavender. Gray line represents the spike detection threshold. ***B***, Representative traces showing the recording of waveforms on each of the tetrode channels for Unit A (left) and Unit B (right). Autocorrelations for each unit are shown below. ***C***, The three-dimensional projections of the feature vectors of Unit A and Unit B in wavelet coefficients 1, 7, and 3. For the details of the spike-sorting software and analysis see Materials and Methods. ***D***, Histogram of spontaneous firing rates for all well isolated units in the mPFC. The overall distribution of spontaneous firing rates showed approximately two peaks and was best fit with two Gaussians (red curves). We separated units into putative PNs (firing rates, <3 Hz) and INs (firing rates, >3 Hz). ***E***, PNs had significantly higher levels of bursting activity than INs (10.23 ± 0.21 vs 7.77 ± 0.26; two-sided Mann–Whitney test, Mann–Whitney $U = 426$; ****$p < 0.0001$), but did not differ significantly in spike width (0.148 ± 0.003 vs 0.151 ± 0.003 ms; two-sided Mann–Whitney test: Mann–Whitney $U = 1449$, $p > 0.05$). ***F***, Proportions of PNs and INs from the mPFC sorted during training (top) and test (bottom) sessions. ***G***, Left, Representative cross-correlogram between a putative PN and another neuron showing a short-latency, presumably monosynaptic excitatory interaction. Right, Representative cross-correlogram between a putative IN and another neuron showing a gap, possibly monosynaptic, inhibitory interaction. Reference events correspond to the spikes of the presynaptic neuron (bins, 0.5 ms). Triangle, PN; circle, IN; squares, other neurons. ***H***, Placement of tetrode tips in the mPFC of all rats performing NOR task.

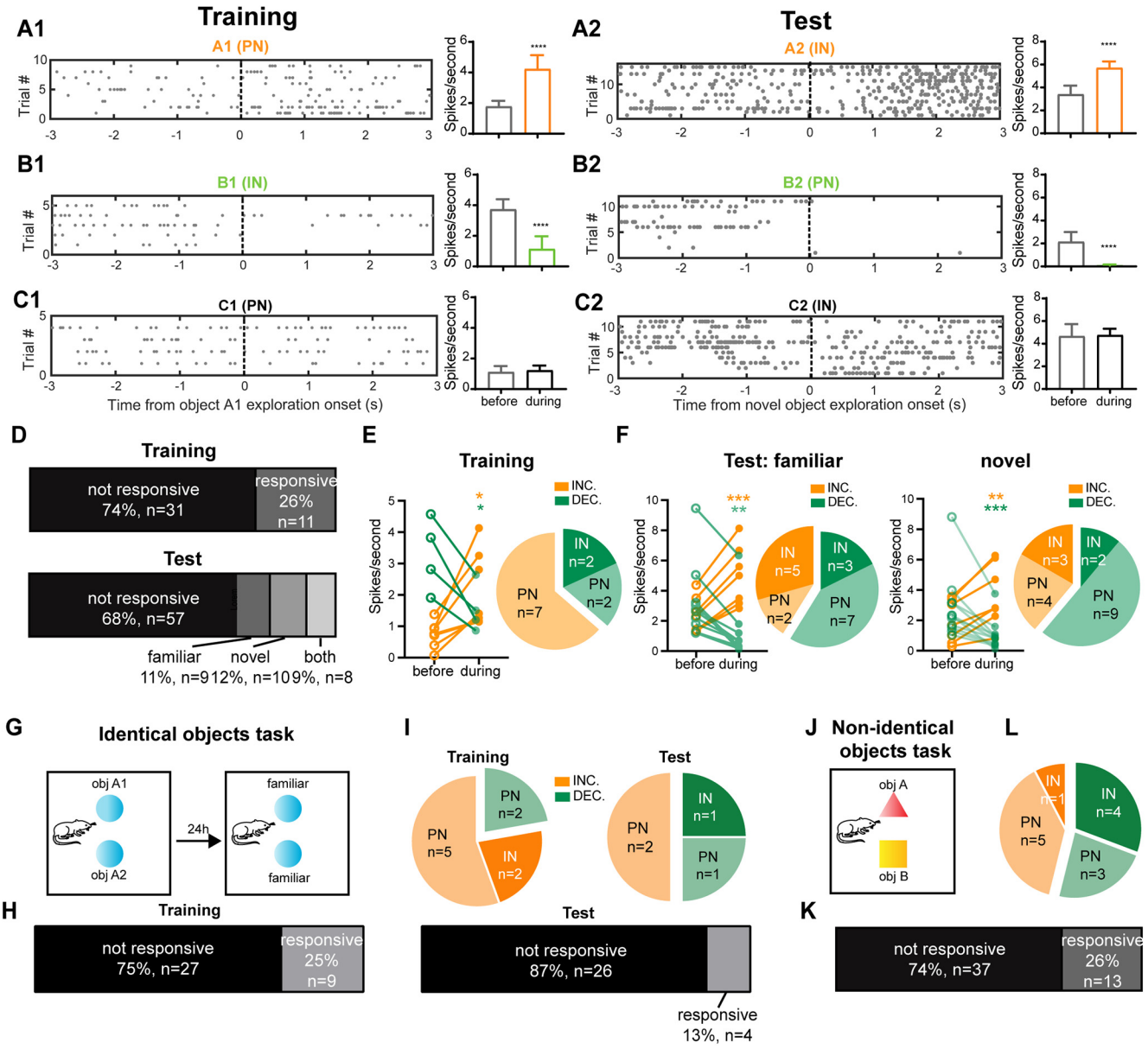

Figure 6. Principal neurons and interneurons in the mPFC respond to objects differently during NOR training and test sessions. ***A1***, ***B1***, ***C1***, Three representative neurons showing an increase (PN, ****$p < 0.0001$, $n = 9$ trials; ***A1***), a decrease (IN, ****$p < 0.0001$, $n = 5$ trials; ***B1***), or no change (PN, $p > 0.05$, $n = 4$ trials; ***C1***) in discharge during object exploration in the training session. Left, Raster plot of individual spike times with each row representing a trial. Right, Mean firing rates across the trials, mean ± SEM. Time zero marks the start of object exploration. All the tests are two-sided Wilcoxon rank-sum tests. ***A2***, ***B2***, ***C2***, Representative responses of three neurons during the test session showing an increase (IN, ****$p < 0.0001$, $n = 15$ trials; ***A2***), a decrease (PN, ****$p < 0.0001$, $n = 11$ trials; ***B2***), or no response (IN, $p > 0.05$, $n = 11$ trials; ***C2***) to object exploration. Left, raster plot of individual spike times with each row representing a trial; right, mean firing rates across the trials. Values are the mean ± SEM. All tests are two-sided Wilcoxon rank-sum tests. ***D***, Top, Percentages of object-responsive neurons during training ($n = 42$); bottom, during testing ($n = 84$). ***E***, Scatter plot shows the response of neurons during exploration of objects. Neurons in the mPFC respond by either increasing (orange, INC.) or decreasing (green, DEC.) their discharge rate (two-sided Wilcoxon matched-pairs signed-rank test, INC: *$p < 0.05$, $n = 7$ cells; paired two-sided t test, DEC: $t_3 = 4.933$, *$p < 0.05$, $n = 4$ cells). The pie chart on the right separates responsive cells into PNs and INs. ***F***, Response of neurons to familiar (left) and novel (right) objects during the test session. Scatter plots shows the response of neurons during exploration of familiar (left) and novel (right) objects (familiar object responsive; paired two-sided t test, INC.: $t_{(6)} = 8.298$, ***$p < 0.001$, $n = 7$ cells; two-sided Wilcoxon matched-pairs signed-rank test, DEC.: **$p < 0.01$, $n = 10$ cells; novel object responsive: paired two-sided t test, INC.: $t_{(6)} = 5.814$, **$p < 0.01$, $n = 7$ cells; two-sided Wilcoxon matched-pairs signed-rank test, DEC.: ***$p < 0.001$, $n = 11$ cells). The pie charts separate responsive cells into PNs and INs for response to familiar (left) and novel (right) objects. ***G***, Schematic of the identical objects task. ***H***, Numbers of mPFC object-responsive neurons during the identical objects task training (left) and test (right) sessions. ***I***, Pie charts show the proportions PNs and INs that respond during object exploration by increasing (orange, INC.) or decreasing (green, DEC.) their firing rate (two-sided Wilcoxon matched-pairs signed-rank test) in the identical objects task. ***J***, Schematic of the nonidentical objects task. ***K***, Numbers of mPFC object-responsive neurons during the nonidentical objects task. ***L***, Pie charts show the proportions PNs and INs that respond during object exploration by increasing (orange, INC.) or decreasing (green, DEC.) their firing rate (two-sided Wilcoxon matched-pairs signed-rank test) in the nonidentical objects task.

task test session (Fig. 6*D*, bottom). Furthermore, we did not see a trend of increased discharge of INs and a decreased discharge of PNs (Fig. 6*I*, right) as seen in the NOR test session (Fig. 6*F*). This result is consistent with our c-Fos study, which shows significantly fewer c-Fos-positive cells in the mPFC in the control group, exposed to two familiar objects compared with the NOR group (Fig. 1*H*, top, *J*, left). This result suggests that following a single training session, rats remember the identity of the objects present and respond robustly to the presence of a novel object. That is, rats spent

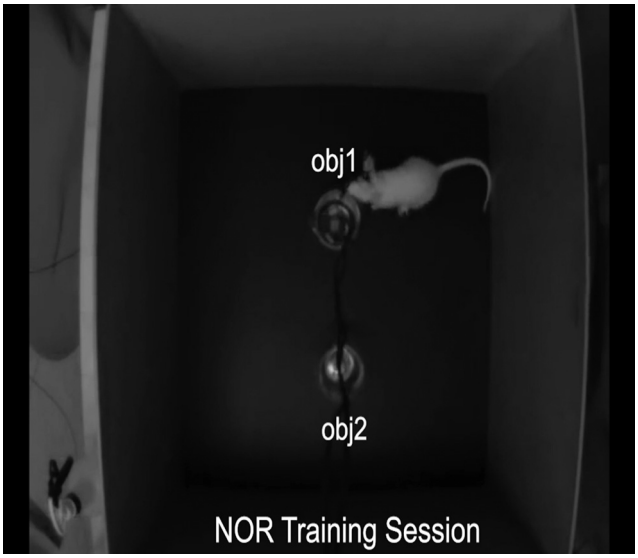

Movie 1. Some neurons in the mPFC increase their discharge during object exploration. The movie shows an animal as it explores two objects in the environment. A tetrode has been placed in the mPFC, and each click in the audio represents one firing event of the neuron. [View online]

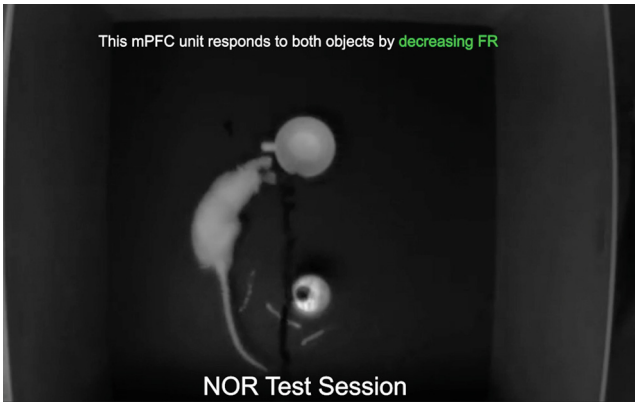

Movie 2. Some neurons in the mPFC decrease their discharge during object exploration. The movie shows an animal as it explores novel and familiar objects in the environment. A tetrode has been placed in the mPFC, and each click in the audio represents one firing event of the neuron. [View online]

more time exploring the novel object (Fig. 1*B*) and more neurons in the mPFC are responsive when a novel object is present (Figs. 1*H*,*J*, 6*F*,*H*).

Finally, to test whether the activity of PNs and INs during the NOR test session may be because of nonmnemonic aspects of object discrimination, such as object shape, rats were exposed to two distinct novel objects (Fig. 6*J*), with no training session. With this paradigm, we identified 13 of 50 object-responsive units (26%; Fig. 6*K*). We found that five of eight responsive mPFC PNs (63%) increased their firing rate, and four of five mPFC INs reduced their firing during object exploration (Fig. 6*L*). The mPFC single-unit dynamics of this nonidentical objects task is similar to that of the NOR training session, where PNs tended to increase their firing rates (Fig. 6*E*) but were distinct from those of the NOR test session where PNs tended to decrease their firing rates and a large proportion of neurons with increases in firing rate were INs (Fig. 6*F*), suggesting that the change in single-unit dynamics in the NOR test session is indeed relevant to recognition memory and not simply to object discrimination.

HPC–mPFC input is required for NOR

We have shown that during NOR there is an increase in overall power and temporal coupling of theta oscillations in the HPC and mPFC with the HPC leading the mPFC. Together with evidence that the HPC forms strong excitatory projections to the mPFC (Hoover and Vertes, 2007; Marek et al., 2018), and the fact that the discharge of neurons in the mPFC is object responsive during NOR, we hypothesized that the coupled activity is driven by HPC projections to the mPFC and required for NOR. To test this hypothesis, we optogenetically silenced the projection from the HPC to the mPFC. AAV carrying ArchT-GFP (green fluorescent protein) was delivered bilaterally into the CA1 region of the HPC (Fig. 7*A*), and optical fibers were implanted in the mPFC to inhibit axon terminals of HPC input to the mPFC (ArchT group; Fig. 7*B*). Control animals received bilateral AAV-eYFP injections into the same region of the HPC. Animals then underwent the NOR task, with HPC terminals in the mPFC being silenced using intermittent green laser light (561 nm) stimulation during the NOR test session (1 min on/1 min off; Fig. 7*C*).

Delivery of green light to the mPFC in animals expressing ArchT, effectively silencing transmitter release from HPC inputs, significantly reduced the ability of animals to distinguish novel from familiar objects, as indicated by a reduced object discrimination index during the light-on phase compared with the light-off phase but had no effect in the control group (Fig. 7*D*,*E*). Silencing this pathway did not change the total exploration time of animals in either the ArchT group or the sham-stimulated control group (Fig. 7*F*). There was no effect on the familiar object exploration time (Fig. 7*G*, left), indicating that the effects of light stimulation were not because of an overall reduction in exploratory behavior. However, this manipulation significantly reduced the novel object exploration time of the rats (Fig. 7*G*, right), with no change in the distance traveled and velocity of the animals (Fig. 7*H*). Importantly, simultaneous LFP recordings revealed that theta coupling between the HPC and mPFC was significantly reduced by inhibiting the HPC → mPFC projection during NOR, with theta coupling being unaffected during familiar objection exploration (Fig. 7*I*, left). No change in HPC–mPFC theta coupling was observed between the light-on and light-off phases during either familiar or novel object exploration in the sham-stimulated control group (Fig. 7*I*, right).

Discussion

Upon entering a new environment, animals spend time exploring and form a cognitive map of the space they are in (McNaughton et al., 2006). The formation and recall of this spatial memory map has largely been attributed to the HPC (Nadel et al., 2012). Experiences in this environment, such as the presence of particular objects, form episodic memories storing what happened and where it happened (Squire et al., 2007). Recall of this memory requires coordinated activity between the HPC and prefrontal cortex (Eichenbaum, 2000, 2017; Orsini et al., 2011). On returning to the same environment, a change in either the location of previously encountered objects or the presence of new objects evokes an attentive reflex allowing animals to discriminate novel from familiar objects (Warburton and Brown, 2015). Lesion studies have established that this process of novel object recognition engages a large network that includes the HPC, PRh, and mPFC (Mumby, 2001; Barker and Warburton, 2011; Morici et al., 2015; Warburton and Brown, 2015). We have shown that effective NOR

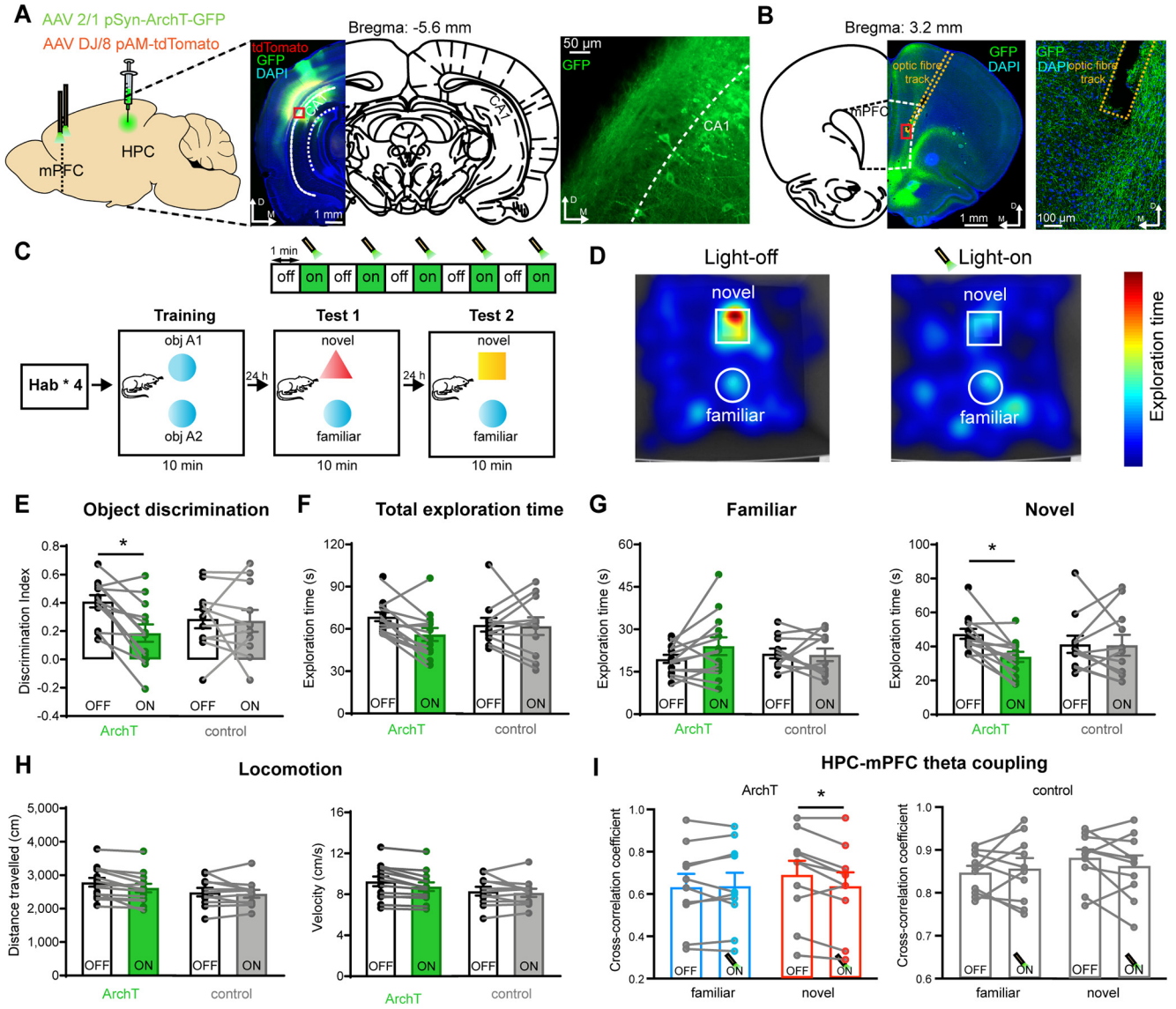

Figure 7. HPC input to the mPFC is required for theta coupling and recognition memory. ***A***, Experimental paradigm. AAV expressing ArchT-GFP was delivered to the CA1 HPC with tdTomato as the marker. Picture on the right show transduced pyramidal neurons in area CA1 of the indicated region (red square). ***B***, Images show terminal GFP labeling in the mPFC at the indicated bregma. ***C***, Schematic shows the behavioral task during training and test. The HPC-to-mPFC input was inhibited during the two NOR tests with 1 min bins (light-on/light-off cycle). ***D***, Heat maps of the exploratory behavior of a representative rat (with ArchT expression) during the light-off (left) and light-on (right) phases in the NOR test session. ***E***, The discrimination index was significantly reduced by light stimulation in the ArchT group (two-way ANOVA with Bonferroni's multiple-comparison test: ArchT group: $^*p < 0.05$, $N = 13$; control group: $p > 0.05$, $N = 11$) during the light-on phases. ***F***, The total object exploration time in the Arch group and control group (two-way ANOVA with Bonferroni's multiple-comparison test: ArchT group: $p > 0.05$, $N = 13$; control group: $p > 0.05$, $N = 11$). ***G***, The familiar exploration time (left) did not change between the light-off and light-on phases (two-way ANOVA with Bonferroni's multiple-comparison test: ArchT group: $p > 0.05$, $N = 13$; control group: $p > 0.05$, $N = 11$), but the novel object exploration time (right) was significantly reduced during the light-on phases (two-way ANOVA with Bonferroni's multiple-comparison test: ArchT group: $^*p < 0.05$, $N = 13$; control group: $p > 0.05$, $N = 11$). ***H***, The distance traveled (left) and velocity (right) during the light-off and light-on phases (two-way ANOVA with Bonferroni's multiple-comparison test: ArchT group: distance traveled, $p > 0.05$, $N = 13$; control group: distance traveled, $p > 0,05$, $N = 11$; velocity, $p > 0.05$, $N = 11$). ***I***, Left, Inhibiting the HPC → mPFC projection did not change HPC–mPFC theta coupling during familiar object exploration but significantly reduced HPC–mPFC theta coupling during NOR in the ArchT group (three-way ANOVA with Bonferroni's multiple-comparison test; ArchT group: familiar object, $p > 0.05$, $n = 10$ test sessions; novel object, $^*p < 0.05$, $n = 10$ test sessions; control group: familiar object, $p > 0.05$, $n = 10$ test sessions; novel object, $p > 0.05$, $n = 10$ test sessions). Values are the mean ± SEM. *N* represents the number of rats.

requires coupled theta activity between the HPC and mPFC and is driven by synaptic input from the HPC to the mPFC.

Using an object recognition behavioral task, and c-Fos as a marker of neural activity, we first show that NOR engages neurons in the mPFC and CA1 region of the HPC (Fig. 1). These results are in agreement with studies that identified increased c-Fos expression in either the mPFC or HPC following NOR (Rinaldi et al., 2010; Barbosa et al., 2013; Melani et al., 2017; Tanimizu et al., 2018; Cinalli et al., 2020). Similarly, other IEGs, such as ZIF-68 and ARC, markers for neuronal activity and plasticity, are also increased in mPFC/HPC CA1 with NOR (Barbosa et al., 2013; Cinalli et al., 2020). Of particular relevance to the current study is that interregional correlations of c-Fos expression have been demonstrated between HPC and mPFC, suggesting enhanced neural connectivity between these structures following NOR (Tanimizu et al., 2018). Supporting this suggestion, simultaneous electrophysiological recordings in the mPFC and ventral HPC revealed that oscillatory theta activity in these structures is enhanced during NOR (Fig. 3). During testing, theta power was higher during recognition of the novel object,

with NOR performance correlated with the enhanced LFP power during novel object exploration. Notably, during training, theta power in the HPC did not change during object exploration compared with the resting state, showing that enhanced theta power during NOR is not because of motor behaviors such as whisking and sniffing. Although object exploration enhanced overall LFP power during NOR training in the mPFC, only theta was significantly upregulated in both the mPFC and HPC during novel object exploration compared with familiar object exploration in the NOR test session. Moreover, theta oscillations in the HPC and mPFC were highly coupled during NOR, with the HPC leading the mPFC (Fig. 4*D*,*E*), suggesting that synchronized neural activity between these regions is critical for novelty discrimination. Pyramidal neurons in the HPC send a direct projection mPFC (Hoover and Vertes, 2007; Parent et al., 2010; Marek et al., 2018), and optogenetically silencing this input to the mPFC reversibly disrupted coupled theta activity and the ability of animals to recognize and respond to novel objects (Fig. 7). This suggests that object-relevant information is distributed from the HPC to the mPFC.

Synchronized theta activity between the PFC and HPC has been shown during behavioral tasks that require memory retrieval, in both animals (Liu et al., 2018; Zielinski et al., 2019) and humans (Minxha et al., 2020). Single-unit recordings from neurons in the mPFC have shown a diversity of activity changes during memory tasks (Hyman et al., 2010). Moreover, this activity in the mPFC entrains theta oscillations (Abbas et al., 2018). Similarly, we find that both PNs and INs in the mPFC are driven during initial object exploration; however, the overall fraction of responsive INs is larger during the NOR session. Moreover, while INs largely increase their discharge in NOR, PNs are inhibited. The primary target of HPC input to the mPFC is parvalbumin-positive interneurons, leading to inhibition of principal neuron activity (Marek et al., 2018). Thus, we suggest that that drive in the activity of INs and the inhibition of PNs during recognition memory retrieval (NOR test session) is mediated by direct HPC projection to the mPFC. Given that PV^+-INs play a critical role in regulating neural oscillations to promote synaptic plasticity and memory formation (Ognjanovski et al., 2017), it is plausible that hippocampal entrainment of prefrontal neural activity through PV^+-INs synchronize the two brain regions to facilitate NOR. However, additional experiments are required to fully unravel how the underlying increase in coupled theta activity drives single-unit activity and to explore the role of particular neural subtypes in regulating novelty discrimination.

It should also be noted that the dorsal-to-ventral poles of the CA1 differ in their anatomic projections, electrophysiological properties, molecular markers, and behavioral functions (Fanselow and Dong, 2010; Wu et al., 2015). While chemogenetic inactivation of dorsal HPC prevents NOR (Tuscher et al., 2018), it does not project directly to the mPFC, and must therefore regulate NOR via other brain structures, such as perirhinal cortex (Jay and Witter, 1991; Verwer et al., 1997; Cenquizca and Swanson, 2007; Hoover and Vertes, 2007). The dHPC may also regulate the function of more ventral hippocampal locations, such as the recording site of this study, via longitudinal projections (Wu et al., 2015) or by theta "traveling waves," which advance in a dorsoventral direction across the HPC during spatial tasks in rats (Lubenov and Siapas, 2009; Patel et al., 2012). Thus, during NOR, it is likely that that recordings in the dorsal hippocampus would also be correlated with those in the mPFC; however, we expect that the phase delay between the two would be longer.

Together, our results reveal that the mPFC and HPC are recruited during NOR, providing new evidence for the HPC–mPFC theta LFP temporal coupling in this task. These findings further establish the roles of the mPFC and HPC in object recognition memory and provide clear evidence that the direct HPC → mPFC projection is essential for object recognition memory. Our findings also support the general notion that retrieval and updating of a memory are both HPC and mPFC dependent (Nadel et al., 2012). Furthermore, these results highlight theta-band temporal coupling as a neural correlate of recognition memory and suggest that memory-related interactions between the HPC and mPFC require coherence in theta-band oscillations, in accordance with emerging concepts regarding the role of theta oscillations in memory-guided behavior at a circuit level (Berens and Horner, 2017). The predominant recruitment of local interneurons in the mPFC during NOR highlights the key role of these cells in synchronized network oscillation (Buzsáki and Draguhn, 2004; Wang, 2010). These insights into the mechanism by which the HPC and mPFC interact to contribute to memory further our understanding of the neurobiological basis of recognition memory and provide a foundation for theories on how dysfunction in this system contributes to cognitive disorders. A number of psychiatric disorders including schizophrenia, Alzheimer's disease, and depression are characterized by abnormal HPC–PFC communication, abnormal theta oscillation, and memory deficits (Zangbar et al., 2020). Thus, this study may also have implications for the development of novel circuit-based therapeutic interventions for these disorders.

References

Abbas AI, Sundiang MJM, Henoch B, Morton MP, Bolkan SS, Park AJ, Harris AZ, Kellendonk C, Gordon JA (2018) Somatostatin interneurons facilitate hippocampal-prefrontal synchrony and prefrontal spatial encoding. Neuron 100:926–939.e3.

Akirav I, Maroun M (2006) Ventromedial prefrontal cortex is obligatory for consolidation and reconsolidation of object recognition memory. Cereb Cortex 16:1759–1765.

Baker KB, Kim JJ (2002) Effects of stress and hippocampal NMDA receptor antagonism on recognition memory in rats. Learn Mem 9:58–65.

Barbosa FF, Santos JR, Meurer YS, Macêdo PT, Ferreira LM, Pontes IM, Ribeiro AM, Silva RH (2013) Differential cortical c-Fos and Zif-268 expression after object and spatial memory processing in a standard or episodic-like object recognition task. Front Behav Neurosci 7:112.

Barker GR, Warburton EC (2011) When is the hippocampus involved in recognition memory? J Neurosci 31:10721–10731.

Barker GR, Bird F, Alexander V, Warburton EC (2007) Recognition memory for objects, place, and temporal order: a disconnection analysis of the role of the medial prefrontal cortex and perirhinal cortex. J Neurosci 27:2948–2957.

Barker GR, Banks PJ, Scott H, Ralph GS, Mitrophanous KA, Wong LF, Bashir ZI, Uney JB, Warburton EC (2017) Separate elements of episodic memory subserved by distinct hippocampal-prefrontal connections. Nat Neurosci 20:242–250.

Barnett L, Seth AK (2014) The MVGC multivariate Granger causality toolbox: a new approach to Granger-causal inference. J Neurosci Methods 223:50–68.

Berens SC, Horner AJ (2017) Theta rhythm: temporal glue for episodic memory. Curr Biol 27:R1110–R1112.

Bevins RA, Besheer J (2006) Object recognition in rats and mice: a one-trial non-matching-to-sample learning task to study 'recognition memory'. Nat Protoc 1:1306–1311.

Blatt M, Wiseman S, Domany E (1996) Superparamagnetic clustering of data. Phys Rev Lett 76:3251–3254.

Buzsáki G (2006) Rhythms of the brain. Oxford: Oxford UP.

Buzsáki G, Draguhn A (2004) Neuronal oscillations in cortical networks. Science 304:1926–1929.

Buzsáki G, Anastassiou CA, Koch C (2012) The origin of extracellular fields and currents–EEG, ECoG, LFP and spikes. Nat Rev Neurosci 13:407–420.

Cenquizca LA, Swanson LW (2007) Spatial organization of direct hippocampal field CA1 axonal projections to the rest of the cerebral cortex. Brain Res Rev 56:1–26.

Cinalli DA Jr, Cohen SJ, Guthrie K, Stackman RW Jr (2020) Object recognition memory: distinct yet complementary roles of the mouse CA1 and perirhinal cortex. Front Mol Neurosci 13:527543.

Clark RE, Zola SM, Squire LR (2000) Impaired recognition memory in rats after damage to the hippocampus. J Neurosci 20:8853–8860.

Clarke JR, Cammarota M, Gruart A, Izquierdo I, Delgado-García JM (2010) Plastic modifications induced by object recognition memory processing. Proc Natl Acad Sci U S A 107:2652–2657.

Cohen SJ, Munchow AH, Rios LM, Zhang G, Asgeirsdóttir HN, Stackman RW Jr (2013) The rodent hippocampus is essential for nonspatial object memory. Curr Biol 23:1685–1690.

Csicsvari J, Hirase H, Czurko A, Buzsáki G (1998) Reliability and state dependence of pyramidal cell-interneuron synapses in the hippocampus: an ensemble approach in the behaving rat. Neuron 21:179–189.

Eichenbaum H (2000) A cortical-hippocampal system for declarative memory. Nat Rev Neurosci 1:41–50.

Eichenbaum H (2017) Prefrontal-hippocampal interactions in episodic memory. Nat Rev Neurosci 18:547–558.

Ennaceur A, Delacour J (1988) A new one-trial test for neurobiological studies of memory in rats. 1: behavioral data. Behav Brain Res 31:47–59.

Fanselow MS, Dong HW (2010) Are the dorsal and ventral hippocampus functionally distinct structures? Neuron 65:7–19.

Furlong TM, Richardson R, McNally GP (2016) Habituation and extinction of fear recruit overlapping forebrain structures. Neurobiol Learn Mem 128:7–16.

Hammond RS, Tull LE, Stackman RW (2004) On the delay-dependent involvement of the hippocampus in object recognition memory. Neurobiol Learn Mem 82:26–34.

Herrera DG, Robertson HA (1996) Activation of c-fos in the brain. Prog Neurobiol 50:83–107.

Hoover WB, Vertes RP (2007) Anatomical analysis of afferent projections to the medial prefrontal cortex in the rat. Brain Struct Funct 212:149–179.

Hyman JM, Zilli EA, Paley AM, Hasselmo ME (2010) Working memory performance correlates with prefrontal-hippocampal theta interactions but not with prefrontal neuron firing rates. Front Integr Neurosci 4:2.

Iwamura E, Yamada K, Ichitani Y (2016) Involvement of hippocampal NMDA receptors in retrieval of spontaneous object recognition memory in rats. Behav Brain Res 307:92–99.

Jay TM, Witter MP (1991) Distribution of hippocampal CA1 and subicular efferents in the prefrontal cortex of the rat studied by means of anterograde transport of Phaseolus vulgaris-leucoagglutinin. J Comp Neurol 313:574–586.

Jones MW, Wilson MA (2005) Theta rhythms coordinate hippocampal-prefrontal interactions in a spatial memory task. PLoS Biol 3:e402.

Liu T, Bai W, Xia M, Tian X (2018) Directional hippocampal-prefrontal interactions during working memory. Behav Brain Res 338:1–8.

Lubenov EV, Siapas AG (2009) Hippocampal theta oscillations are travelling waves. Nature 459:534–539.

Manns JR, Hopkins RO, Reed JM, Kitchener EG, Squire LR (2003) Recognition memory and the human hippocampus. Neuron 37:171–180.

Marek R, Jin J, Goode TD, Giustino TF, Wang Q, Acca GM, Holehonnur R, Ploski JE, Fitzgerald PJ, Lynagh T, Lynch JW, Maren S, Sah P (2018) Hippocampus-driven feed-forward inhibition of the prefrontal cortex mediates relapse of extinguished fear. Nat Neurosci 21:384–392.

McNaughton BL, Battaglia FP, Jensen O, Moser EI, Moser MB (2006) Path integration and the neural basis of the "cognitive map". Nat Rev Neurosci 7:663–678.

Melani R, Chelini G, Cenni MC, Berardi N (2017) Enriched environment effects on remote object recognition memory. Neuroscience 352:296–305.

Merkow MB, Burke JF, Kahana MJ (2015) The human hippocampus contributes to both the recollection and familiarity components of recognition memory. Proc Natl Acad Sci U S A 112:14378–14383.

Minxha J, Adolphs R, Fusi S, Mamelak AN, Rutishauser U (2020) Flexible recruitment of memory-based choice representations by the human medial frontal cortex. Science 368:eaba3313.

Miranda M, Kent BA, Morici JF, Gallo F, Saksida LM, Bussey TJ, Weisstaub N, Bekinschtein P (2018) NMDA receptors and BDNF are necessary for discrimination of overlapping spatial and nonspatial memories in perirhinal cortex and hippocampus. Neurobiol Learn Mem 155:337–343.

Morici JF, Bekinschtein P, Weisstaub NV (2015) Medial prefrontal cortex role in recognition memory in rodents. Behav Brain Res 292:241–251.

Mumby DG (2001) Perspectives on object-recognition memory following hippocampal damage: lessons from studies in rats. Behav Brain Res 127:159–181.

Nadel L, Hupbach A, Gomez R, Newman-Smith K (2012) Memory formation, consolidation and transformation. Neurosci Biobehav Rev 36:1640–1645.

Ognjanovski N, Schaeffer S, Wu J, Mofakham S, Maruyama D, Zochowski M, Aton SJ (2017) Parvalbumin-expressing interneurons coordinate hippocampal network dynamics required for memory consolidation. Nat Commun 8:15039.

Orsini CA, Kim JH, Knapska E, Maren S (2011) Hippocampal and prefrontal projections to the basal amygdala mediate contextual regulation of fear after extinction. J Neurosci 31:17269–17277.

Parent MA, Wang L, Su J, Netoff T, Yuan LL (2010) Identification of the hippocampal input to medial prefrontal cortex in vitro. Cereb Cortex 20:393–403.

Patel J, Fujisawa S, Berényi A, Royer S, Buzsáki G (2012) Traveling theta waves along the entire septotemporal axis of the hippocampus. Neuron 75:410–417.

Paxinos G, Watson C (2007) The rat brain in stereotaxic coordinates, Ed 6. Amsterdam: Academic/Elsevier.

Pezze MA, Marshall HJ, Fone KCF, Cassaday HJ (2015) Dopamine D-1 receptor stimulation modulates the formation and retrieval of novel object recognition memory: role of the prelimbic cortex. Eur Neuropsychopharmacol 25:2145–2156.

Press WH (1992) Numerical recipes in C: the art of scientific computing, Ed 2. Cambridge, UK: Cambridge UP.

Quiroga RQ, Nadasdy Z, Ben-Shaul Y (2004) Unsupervised spike detection and sorting with wavelets and superparamagnetic clustering. Neural Comput 16:1661–1687.

Rinaldi A, Romeo S, Agustín-Pavón C, Oliverio A, Mele A (2010) Distinct patterns of Fos immunoreactivity in striatum and hippocampus induced by different kinds of novelty in mice. Neurobiol Learn Mem 94:373–381.

Siapas AG, Lubenov EV, Wilson MA (2005) Prefrontal phase locking to hippocampal theta oscillations. Neuron 46:141–151.

Smith CN, Jeneson A, Frascino JC, Kirwan CB, Hopkins RO, Squire LR (2014) When recognition memory is independent of hippocampal function. Proc Natl Acad Sci U S A 111:9935–9940.

Squire LR, Wixted JT, Clark RE (2007) Recognition memory and the medial temporal lobe: a new perspective. Nat Rev Neurosci 8:872–883.

Tanimizu T, Kono K, Kida S (2018) Brain networks activated to form object recognition memory. Brain Res Bull 141:27–34.

Tattersall TL, Stratton PG, Coyne TJ, Cook R, Silberstein P, Silburn PA, Windels F, Sah P (2014) Imagined gait modulates neuronal network dynamics in the human pedunculopontine nucleus. Nat Neurosci 17:449–454.

Tuscher JJ, Taxier LR, Fortress AM, Frick KM (2018) Chemogenetic inactivation of the dorsal hippocampus and medial prefrontal cortex, individually and concurrently, impairs object recognition and spatial memory consolidation in female mice. Neurobiol Learn Mem 156:103–116.

Verwer RW, Meijer RJ, Van Uum HF, Witter MP (1997) Collateral projections from the rat hippocampal formation to the lateral and medial prefrontal cortex. Hippocampus 7:397–402.

Wan H, Aggleton JP, Brown MW (1999) Different contributions of the hippocampus and perirhinal cortex to recognition memory. J Neurosci 19:1142–1148.

Wang XJ (2010) Neurophysiological and computational principles of cortical rhythms in cognition. Physiol Rev 90:1195–1268.

Warburton EC, Brown MW (2010) Findings from animals concerning when interactions between perirhinal cortex, hippocampus and medial prefrontal cortex are necessary for recognition memory. Neuropsychologia 48:2262–2272.

Warburton EC, Brown MW (2015) Neural circuitry for rat recognition memory. Behav Brain Res 285:131–139.

Wu MV, Sahay A, Duman RS, Hen R (2015) Functional differentiation of adult-born neurons along the septotemporal axis of the dentate gyrus. Cold Spring Harb Perspect Biol 7:a018978.

Xia F, Richards BA, Tran MM, Josselyn SA, Takehara-Nishiuchi K, Frankland PW (2017) Parvalbumin-positive interneurons mediate neocortical-hippocampal interactions that are necessary for memory consolidation. Elife 6:e27868.

Zangbar HS, Ghadiri T, Vafaee MS, Kalan AE, Fallahi S, Ghorbani M, Shahabi P (2020) Theta oscillations through hippocampal/prefrontal pathway: importance in cognitive performances. Brain Connect 10:157–169.

Zielinski MC, Shin JD, Jadhav SP (2019) Coherent coding of spatial position mediated by theta oscillations in the hippocampus and prefrontal cortex. J Neurosci 39:4550–4565.